Journal of Earth Sciences and Geotechnical Engineering, Vol. 16, No. 2, 2026, 1-15
ISSN: 1792-9040 (print version), 1792-9660 (online)
https://doi.org/10.47260/jesge/1621
Scientific Press International Limited

Geophysical and Geochemical Investigation of Tantalite Mineral Deposits in Laisamis, Marsabit County, Kenya

Ibrahim Koome Ezekiel[1], Odek Antony[1] and Mutie Martin[1]

Abstract

This study investigated tantalite mineralisation in the Laisamis area, Kenya, using integrated geophysical and geochemical methods. Electrical resistivity surveying employed the Schlumberger configuration along four 400 m profiles with 10 m spacing. Resistivity pseudosections revealed that mineralized zones occur within conductive layers ranging from 12–186 Ω · m in the upper 30 m of the subsurface, while high-resistivity bedrock of greater than 2,000 Ω · m marks the lower boundary of mineralisation. These conductive anomalies correspond to weathered troughs and fractured zones within pegmatite bodies hosting tantalite deposits, which are the primary source of tantalum. Geochemical analysis via X-ray fluorescence (XRF) spectrometry confirmed concentrations above 43% in six of ten rock samples, positioning them as high-grade ores. Niobium, iron, and manganese were present as associated elements, with low minor element content indicating clean mineral assemblages favourable for processing. The combination of resistivity imaging and XRF data successfully delineated the spatial extent, depth, and grade of mineralisation. This study demonstrates that integrated geophysical and geochemical methods offer a non-invasive, cost-effective approach for exploring critical metals in underdeveloped regions, supporting sustainable resource development in Kenya.

Keywords: Tantalite, Resistivity, Schlumberger, Pegmatite, Pseudosection, X-ray fluorescence.

[1] Department of Physical Sciences, Chuka University, P.O. Box 109 – 60400, Chuka, Kenya.

Article Info: *Received:* April 5, 2026. *Revised:* June 17, 2026.
Published online: June 30, 2026.

1. Introduction

Tantalum plays a crucial role in modern technologies, including electronics, aerospace and medical devices. It has physical and chemical properties such as excellent electrical conductivity, a high melting point, and resistance to corrosion (Kraft *et al.*, 2021). This rare metal is primarily extracted from tantalite minerals found in pegmatite and placer deposits, which often contain other ores such as columbite, microlite, and wodginite (Simmons *et al*., 2023). Pegmatite rocks rich in tantalum exhibit distinctive electrical resistivity signatures, making geophysical methods valuable for their identification and extraction. However, the global supply of tantalum remains concentrated in a few countries, including Brazil, Australia, and Canada, making the metal vulnerable to supply fluctuations amid growing demand from the technology sector.

In Africa, tantalum production has faced numerous challenges, particularly in the Democratic Republic of Congo, Rwanda, and Nigeria, where artisanal mining, environmental degradation, and geopolitical instability have impacted the industry (Mackay & Simandl, 2014). Kenya's tantalite deposits, notably in the Laisamis area, remain underexplored, but they represent an opportunity to develop supply chains that respect both ethical standards and scientific rigour. Traditional prospecting methods, while culturally significant, often lack the precision required for modern exploration, underscoring the importance of combining indigenous knowledge with advanced geochemical and geophysical techniques such as electrical resistivity profiling, magnetic surveys, and X-ray fluorescence analysis (Ochola, 2021).

The Laisamis region holds considerable untapped mineral wealth, including granitic pegmatites that contain lithium, tantalum, niobium, and rare earth elements. Despite this potential, the area remains underdeveloped, causing Kenya to rely heavily on imports of these critical minerals. Modern geophysical survey methods provide a promising path forward by offering non-invasive, cost-effective ways to map subsurface mineralisation with greater accuracy. These technologies reduce exploration risks and lessen environmental impacts, enabling data-driven decision-making for resource assessment. In doing so, they can unlock economic benefits, promote sustainable mining practices, and support the growth of domestic mineral supply chains through better deposit characterisation.

Tantalite deposits investigation in Laisamis serves as a significant test case for advancing sustainable mineral development in Kenya. The country's efforts to gather geoscientific data align with global best practices, though challenges such as difficult terrain and insufficient infrastructure remain obstacles to full implementation. By confirming and developing these mineral deposits with integrated survey methods, Kenya not only strengthens its domestic industrial base but also positions itself to avoid the issues linked to conflict minerals. This presents an opportunity for Kenya to establish itself as a responsible and ethical supplier in the international market.

The investigation of tantalite mineralisation in Laisamis, which also involved minerals like niobium, manganese, and iron, goes beyond geology. It demonstrates

how resource management in developing countries can balance economic viability with ethical responsibility. By integrating traditional knowledge with modern scientific approaches, Kenya can set an example for equitable and sustainable mineral development. The findings from this study have the potential to attract investment, inform policy, and reduce risks in precious mineral supply chains worldwide. In an era of increasing demand for critical materials such as tantalum, Kenya's strategic approach could serve as a valuable model for other resource-rich regions facing similar challenges.

2. Field measurement

The research employed both the geophysical investigation method of electrical resistivity profiling and the geochemical investigation of samples.

2.1 Electrical resistivity survey

It was carried out in Laisamis, which is located in Marsabit County, in Northern Kenya. Geographically, it lies between latitudes 1° 30'N and 2° 45'N and longitudes 37° 30'E and 38° 30'E.

The ABEM Terrameter LS 2, as shown in Figure 1, is one of the main instruments used for measuring the apparent resistivity of subsurface materials. The Terrameter was connected to the copper electrodes using copper cables to transmit the received electrical current.

Figure 1: ABEM Terrameter and its accessories (Pacanowski *et al.*, 2022).

2.1.1 Electrical data acquisition

The investigation was conducted in selected target areas for electrical resistivity profiling. A 400 m survey profile was carried out, with electrode positions marked every 10 m interval. Copper electrodes were driven into the ground at these locations. Electrical cables connected the electrodes to the ABEM Terrameter, and electrode spacing was measured with a tape measure. The Terrameter, powered by a direct current battery, was switched on and configured with the required survey parameters before data collection began.

Apparent resistivity measurements were recorded along each profile. The readings were displayed in real time and saved digitally for further analysis, while GPS coordinates were also recorded to provide precise location data for each measurement point. The same procedure was repeated along four different profiles in separate locations, allowing for a detailed understanding of the subsurface electrical properties across the study area. This systematic approach ensured accurate and reliable data for interpreting geological structures.

2.1.2 Schlumberger configuration

The Schlumberger configuration is a widely used method in electrical resistivity tomography (ERT) to achieve detailed vertical resolution of the subsurface resistivity distribution. In this setup, electrodes are arranged symmetrically along a survey line, typically at fixed intervals, in this case, 10 m apart. The configuration involves two current electrodes, labelled A and B, placed on the outer edges of the array, while two potential electrodes, M and N, are situated closer together in the centre, as shown in Figure 2.

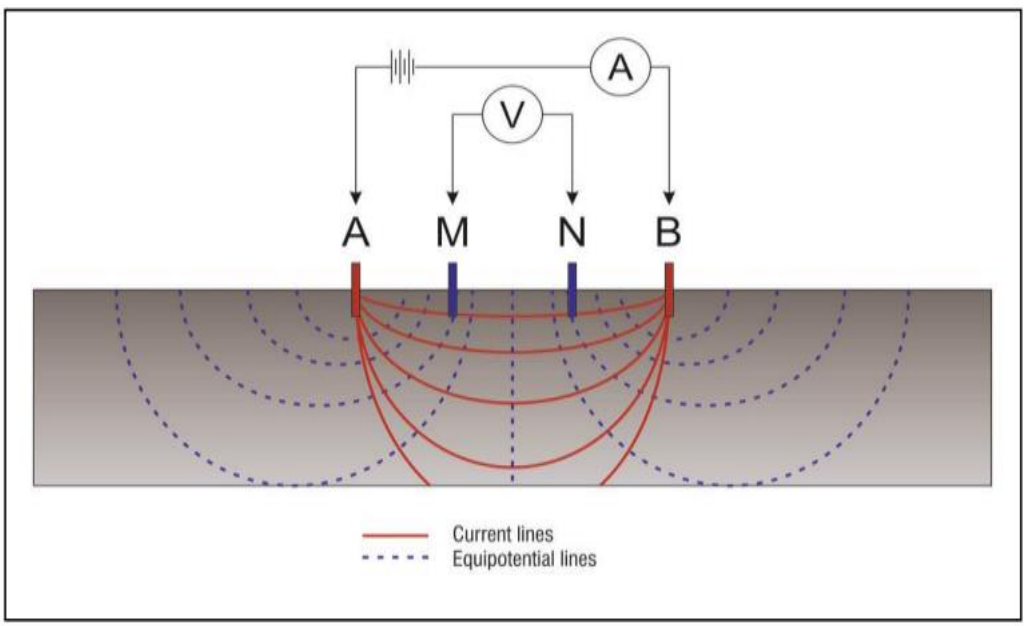

Figure 2: Schlumberger array (Norooz *et al.*, 2024).

The arrangement allows for the injection of electrical current into the ground through the outer electrodes and measurement of the resulting voltage difference between the inner electrodes. The spacing between the current electrodes is varied during the survey to probe different depths while the potential electrodes remain fixed, providing data that helps resolve changes in resistivity with depth. Such flexibility in electrode spacing makes the Schlumberger array effective for mapping vertical variations in subsurface materials.

During the field survey, copper cables connected the electrodes to an electronic instrument called a Terrameter, which controls current injection and measures voltage. The Terrameter was powered on and configured with key parameters, including the number of current cycles and the magnitude of the current injected into the ground. To increase the investigation depth, the outer current electrodes were progressively moved farther apart while keeping the inner potential electrodes stationary. This process, called sounding, continued until the ratio of current to potential electrode spacing became excessively large or voltage measurements dropped below a reliable threshold, ensuring consistent data quality. In this research, four separate profiles were measured within the investigation area, with data from various electrode spacings recorded and saved for further analysis. This systematic measurement procedure enabled the generation of detailed resistivity profiles, aiding in the accurate characterisation of subsurface geological structures.

2.1.3 Electrical resistivity data presentation

Raw electrical resistivity data were cleaned to remove noise and correct errors caused by surface conditions or equipment malfunctions. The processed data were displayed as pseudosections showing measured apparent resistivity, calculated apparent resistivity, and inverse-model resistivity across different electrode spacings and depths. The inversion parameters on the software are shown in Table 1.

Table 1: Inversion parameters.

Parameter category	Parameter name	Value used	Justification
Data quality control	Exterminate bad data points	Removed manually	Spikes were identified via visual inspection of pseudosections and removed prior to inversion.
Inversion damping parameters	Initial damping factor	0.25	The default value of 0.15 produced unstable inversion; therefore, 0.25 was selected.
	Minimum damping factor	0.05	Set to one-fifth of the initial damping factor to maintain stability in deeper layers.
	Damping increase with depth	1.08	Applied to counteract the progressive loss of resolution with depth.
Inversion method	Robust inversion	L1 norm	Selected for its reduced sensitivity to outliers in the moderately noisy dataset.
	Data transformation	Logarithm of apparent resistivity	Applied to accommodate the high resistivity contrast (>20:1) in the study area.
Forward modelling	Horizontal mesh size	4 nodes per electrode	Used to improve forward calculation accuracy over the default 2-node setting.
	Type of forward modelling	Finite-element	Employed for superior accuracy with high resistivity contrasts (>20:1).
	Model refinement	Cell width = 1/2 electrode spacing	Set to half the electrode spacing due to a high-resistivity layer overlying a low-resistivity layer.
Inversion progress	Number of iterations	6	RMS error stabilised after 4 iterations from a maximum of 5.

Using the RES2DINV software, an initial apparent resistivity pseudosection was generated from raw field measurements. This section showed resistivity anomalies, with zones of high or low resistivity corresponding to rock formations or water-bearing layers. Raw data included noise from poor electrode contact, electrical interference, traffic vibrations, or construction activities. Recognising these sources allowed a distinction between geological signals and technical disturbances.

The inversion process computed the root-mean-square error (RMSE) between the observed and calculated apparent resistivity values. The fit quality, expressed as an R^2 value between 0.92 and 0.98, indicated that the modelled resistivity section explained most of the variance in the field data. Noise reduced the signal-to-noise ratio (SNR) below 10 dB. Measurements with SNR > 15 dB were retained for final interpretation.

The calculated pseudosection, derived from the inversion model, predicted the measured data. Comparing this with the observed pseudosection assessed model reliability. A close match between the two confirmed that the model was well-

constrained, ensuring that the subsurface image reflected actual underground conditions.

RES2DINV enabled modelling and interpretation of subsurface resistivity, allowing identification of geological formations. High-resistivity layers indicate bedrock. Fine-tuning inversion parameters and validating results against known geological data reduced artifacts and improved subsurface characterisation. This geophysical analysis provides data for understanding subsurface properties for land-use planning, structural stability assessments, and natural resource management. Characterisation of geological formations supports decision-making, reduces infrastructure risks, and promotes sustainable environmental interaction.

2.2 Geochemical sampling

The initial phase of XRF analysis involved collecting field samples that were representative of the study area. A carefully designed sampling approach by incorporating grid-based, random, and targeted methods guaranteed that the collected materials truly represented the region of interest. Sampling focused on obtaining fresh rock from outcrops. Clean, non-reactive tools, including a stainless-steel trowel and a plastic scoop, were used to collect four samples from depths of 20–50 cm. The remaining six samples were gathered from near the surface and stored appropriately. Each sample's location was recorded using GPS coordinates, along with detailed field notes, before being sealed in chemically inert polypropylene bags to avoid contamination during transport.

Once in the laboratory, the rock samples were air-dried at 40°C for 48 hours to remove moisture without altering their mineralogical makeup. The dried material was then crushed and homogenised in a grinding machine to produce a fine powder with a grain size of less than 75 μm. This powder was mixed with a binding agent and compressed into pellets under high pressure. This preparation step was critical, as both grain size distribution and sample uniformity heavily affect the precision of trace element quantification by X-ray fluorescence (XRF) analysis.

The study used advanced energy-dispersive X-ray fluorescence (ED-XRF) spectrometry as the main method for detecting trace elements. ED-XRF employs semiconductor detectors to sensitively measure trace elements including tantalum (Ta), niobium (Nb), iron (Fe), tin (Sn), tungsten (W) and lithium (Li). The instrument was calibrated using certified reference materials that closely matched tantalite compositions, ensuring quantification accuracy. Detection limits for key trace elements were established between 1 and 5 parts per million (ppm). To uphold analytical precision and reliability, each batch contained duplicate samples, procedural blanks, and certified reference standards. Furthermore, internal standard additions were used to track and correct for matrix effects, which could otherwise compromise the accuracy of XRF measurements.

3. Results

3.1 Geophysical results

Resistivity pseudosections from the survey provide electrical images of the subsurface, reflecting variations in resistivity caused by differences in rock type, moisture content, mineral concentration, porosity, and structural features. Four profiles were conducted using the Schlumberger electrode configuration over 400 m each, with a profile spacing of 10 m apart. The spacing between current electrodes was systematically varied while potential electrodes remained fixed to explore different depths. These profiles enabled the identification of layering, anomalous zones, mineralisation, and formation boundaries.

The pseudosections display three resistivity types. First, measured apparent resistivity provides direct field data that reflects the combined electrical response of subsurface materials. Second, the calculated apparent resistivity is derived from forward modelling based on an assumed resistivity distribution. Third, inverse-model resistivity results from mathematically transforming measured data to estimate true resistivity at depth, thereby revealing rock types, fluid content, and mineralised zones. Together, these three sections enable a direct comparison between raw data and final interpretation, improving the accuracy of identifying geological structures and mineral deposits.

3.1.1 Profile one

In Figure 3, the subsurface is characterised by significant lateral variation. The mineralised zones exhibit resistivity signatures between 14.8 Ω · m and 182 Ω · m. These conductive deposits are situated between the surface depth of 1.25 m and 24.0 m. This profile displays a complex arrangement of intrusions and contrasts, with two massive high-resistivity bodies peaking at 4,275 Ω · m, located on the far left and far right ends of the section. The mineralised zones are found in the transition zone between these two resistive masses. This suggests the mineralisation is controlled by a geological fault or a weathered trough between harder rock units, providing a clear geographical layer where tantalite and associated minerals have accumulated.

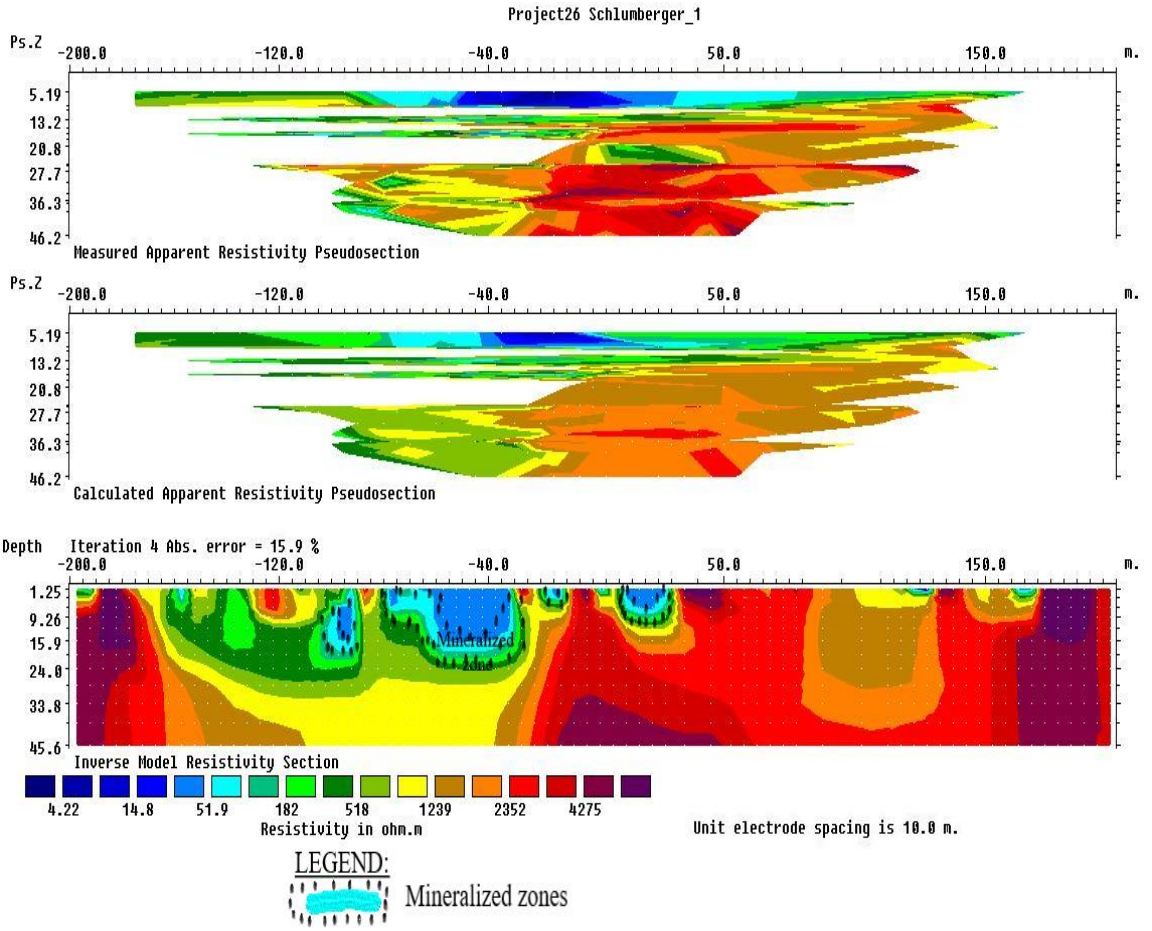

Figure 3: Electrical image for profile one.

3.1.2 Profile two

A well-defined horizontal stratification is as shown in Figure 4. The targeted mineralised zones are found within a broad, continuous conductive layer near the surface, with resistivity values ranging from 16.9 Ω · m to 121 Ω · m. This mineralised geological layer is notably deep in this profile, starting at 1.25 m and extending to a depth of 33.8 m. Below this conductive zone, there is a sharp transition into a high-resistivity layer that begins at a depth of 33.8 m and deepens toward the right, with values reaching 3,761 Ω · m. This contrast indicates that the mineral deposits are hosted within a thick, conductive overburden or weathered zone overlying a dipping, resistive bedrock basement.

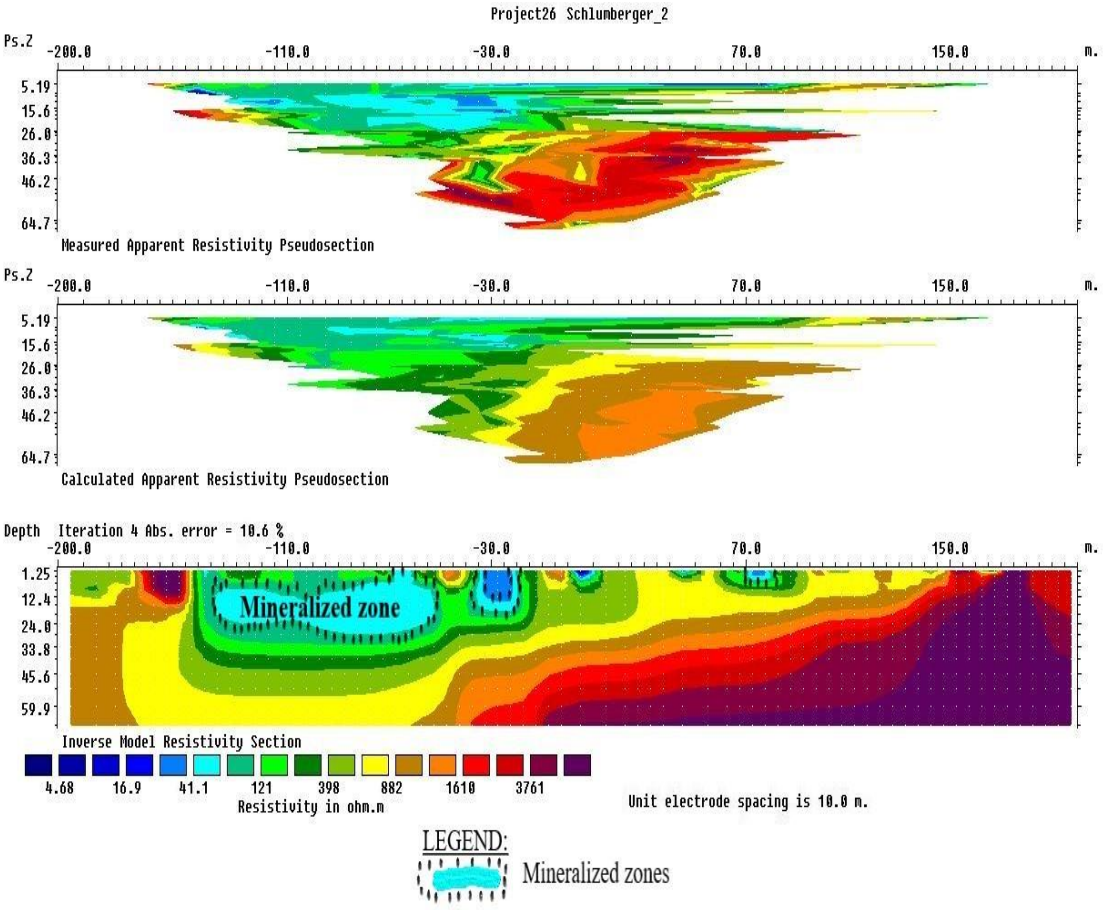

Figure 4: Electrical image for profile two.

3.1.3 Profile three

In Figure 5, the marked mineralised zones are localised within pockets of exceptionally low resistivity, ranging from 12.5 Ω · m to 139 Ω · m. These zones appear as vertical to sub-vertical conductive structures that contrast sharply with the surrounding intermediate layers, which represent resistivity values of between 139 and 477 Ω · m. The primary mineralised features are detected at depths starting from 1.25 m and extending down to approximately 24.0 m. Geologically, these conductive pockets suggest an intrusion-like pattern where mineralised materials have concentrated within a more resistive matrix. At greater depths below 45.6 m, a transition into more competent, higher-resistivity layers of up to 2,947 Ω · m is observed, representing a stable basement or a large-scale hard-rock intrusion.

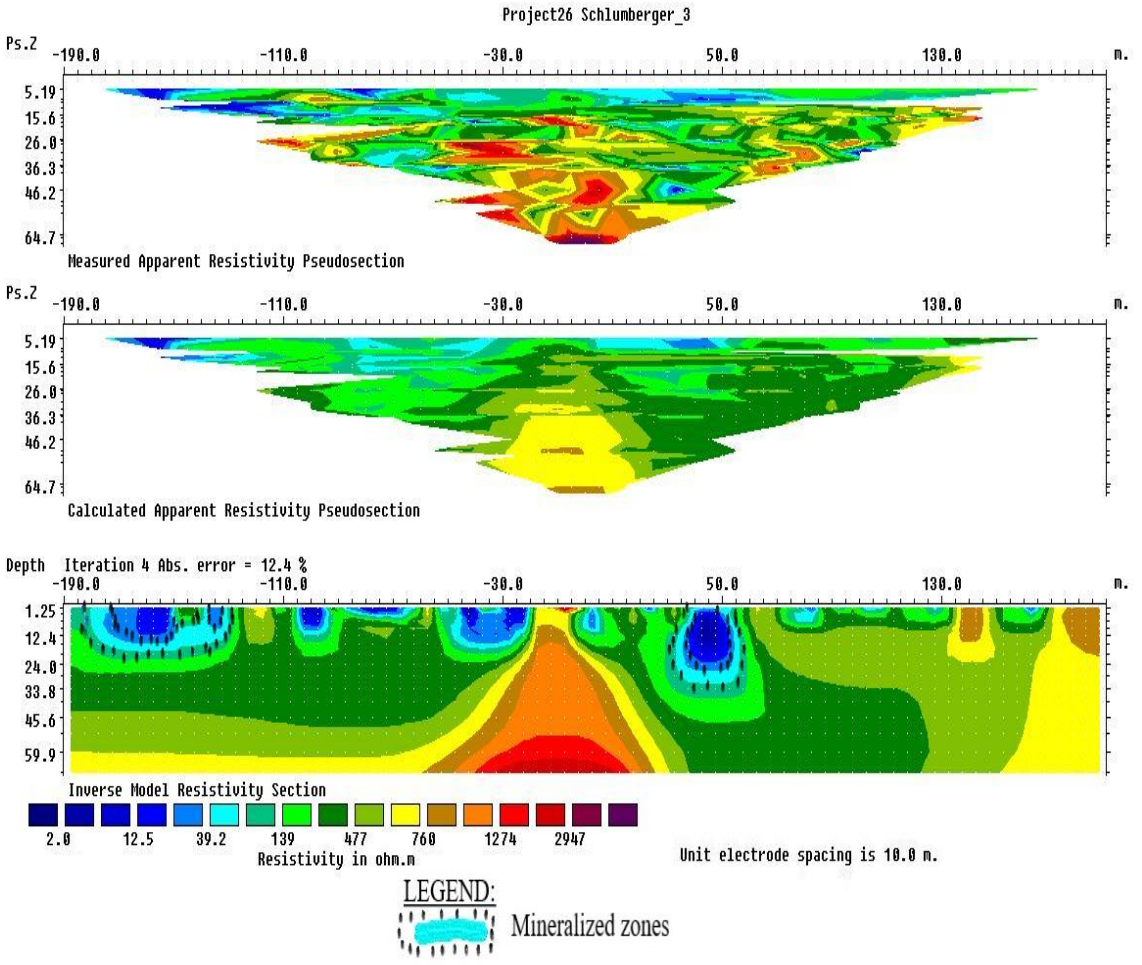

Figure 5: Electrical image for profile three.

3.1.4 Profile four

The profile in Figure 6 reveals a distinct stratigraphic transition. The mineralised zones here are primarily concentrated in the upper sections of the subsurface, characterised by resistivity values between 11.9 Ω · m and 186 Ω · m. These anomalies are most prominent at depths between 1.25 m and 12.4 m, with a significant central feature extending down to 24.0 m. A major geological contrast is visible in this profile where a vast, high-resistivity basement layer, exceeding 2,181 Ω · m, begins abruptly at a depth of around 40 m and remains consistent across the entire section. This creates a clear horizontal transition between a relatively conductive, potentially weathered top layer containing the minerals and a massive, resistive underlying intrusion or bedrock.

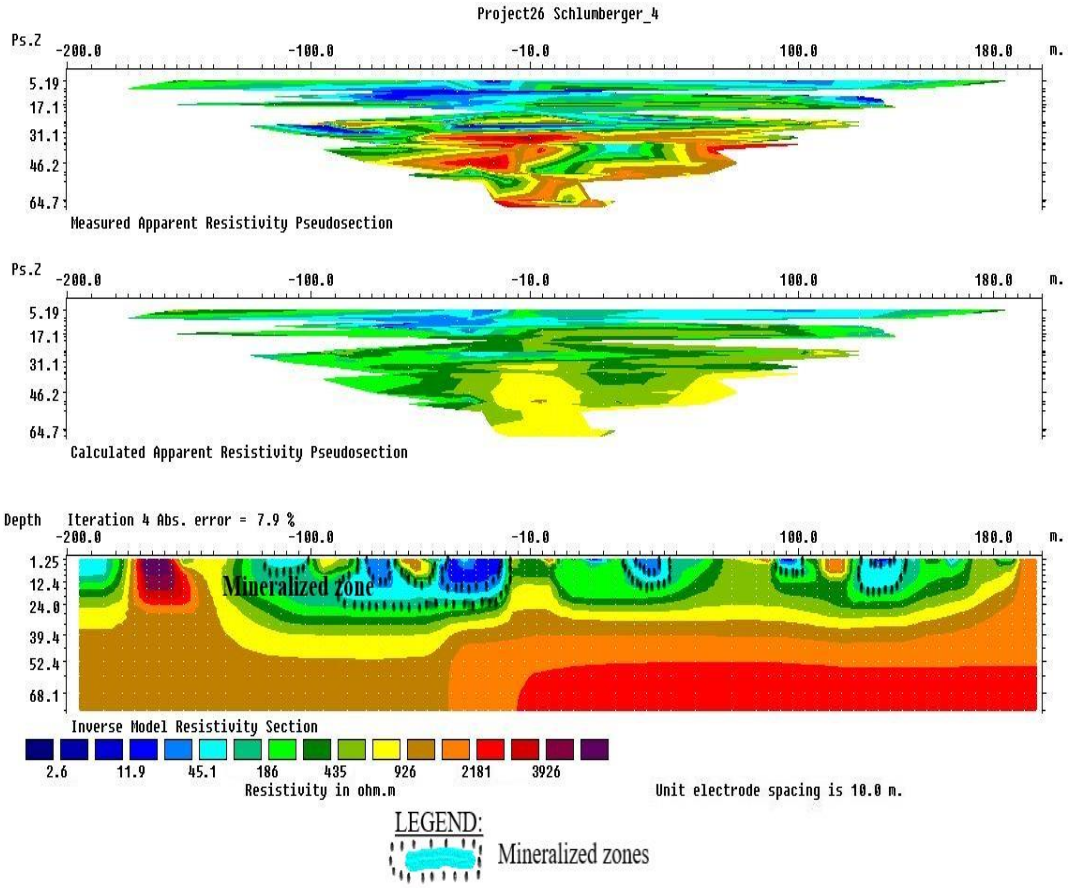

Figure 6: Electrical image for profile four.

Across all profiles, the tantalite deposits are found within the most conductive or low resistivity layers, typically located within a depth of the first 30 meters of the subsurface. The major contrasts are provided by the surrounding bedrock and intrusions, which appear as high-resistivity red and purple zones, marking the geological limits of the mineralised potential in these areas.

3.2 Geochemical results

Ten samples were collected across the 10 km² study area, as shown in Table 2, for systematic elemental analysis using X-ray fluorescence spectrometry (XRF). The samples underwent rigorous preparation, including surface cleaning, fragmentation, pulverisation, and pelletization prior to analysis. A CTX Benchtop XRF spectrometer equipped with Bruker Artax 7 software was employed for precise elemental quantification, with particular attention to tantalite content determination. To ensure data reliability, selected samples served as control standards throughout the analytical process.

Table 2: Sample code description.

Sample Name	Co-ordinates	Sample Type	Landscape
S_1	(1^0 35'N, 37^0 47'E)	Rock	Foot hill
S_2	(1^0 34'N, 37^0 41'E)	Rock debris	Alluvial plain
S_3	(1^0 30'N, 37^0 05'E)	Rock	Hill slope
S_4	(1^0 36'N, 37^0 27'E)	Rock debris	Hill slope
S_5	(1^0 36'N, 37^0 44'E)	Rock	Flat slope
S_6	(1^0 35'N, 37^0 27'E)	Rock	Alluvial plain
S_7	(1^0 37'N, 37^0 15'E)	Rock debris	Flat slope
S_8	(1^0 38'N, 37^0 54'E)	Rock	Alluvial plain
S_9	(1^0 35'N, 37^0 24'E)	Rock debris	Top hill
S_{10}	(1^0 42'N, 37^0 20'E)	Rock	Hill slope

The complete geochemical dataset, including concentrations of tantalite and other elements in the collected samples, is provided in Table 3.

Table 3: Percentage chemical composition of elements in parts per million (ppm) for the samples collected.

Element/Sample	S_1	S_2	S_3	S_4	S_5	S_6	S_7	S_8	S_9	S_{10}
Tantalum (%)	12.96	23.99	45.64	45.51	43.99	16.42	48.01	19.03	57.00	47.12
Niobium (%)	23.50	45.07	14.27	14.91	23.71	35.42	24.00	30.99	28.03	22.00
Manganese (%)	16.58	14.58	14.07	12.38	14.23	24.49	12.25	32.22	5.14	14.90
Iron (%)	45.90	12.46	12.70	14.58	14.14	21.16	12.52	13.75	5.99	12.06
Others (%)	1.06	3.99	13.32	12.72	3.94	2.51	3.22	4.02	3.84	3.92

All the samples indicate a mixture of tantalite deposits that have mainly tantalum, niobium, manganese and iron. The presence of tantalum raises the possibility of large-scale accumulation in valleys with pegmatite rocks.

A graphical presentation of the comparative chemical composition of major elements in the obtained samples is shown in Figure 7.

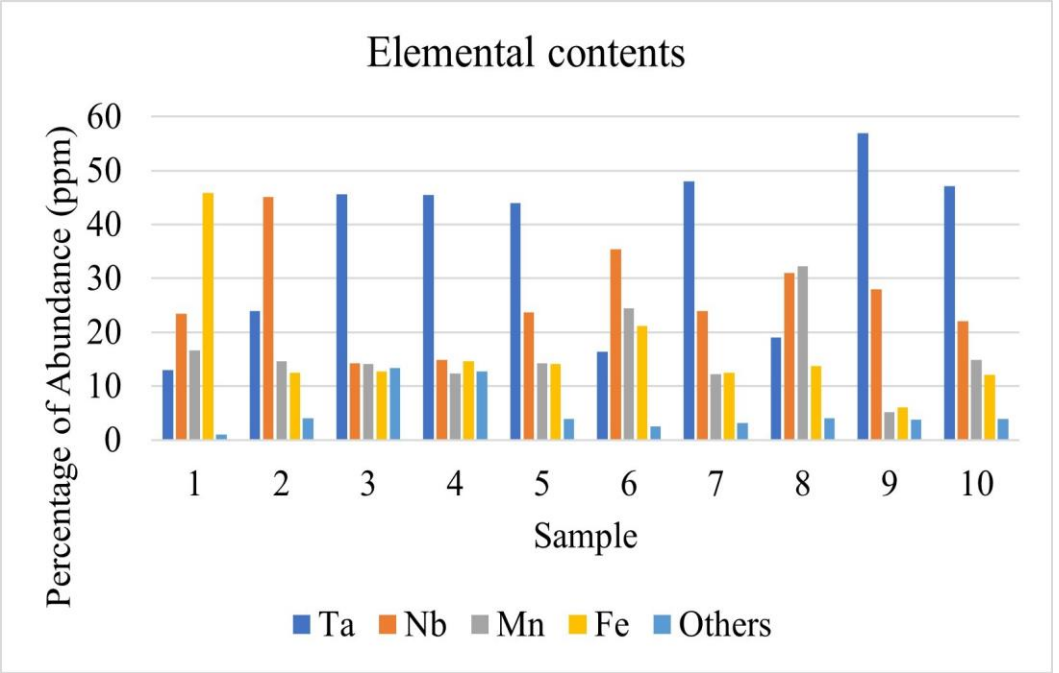

Figure 7: Geochemical composition of all 10 samples done by XRF.

The chemical compositions show significant variation in tantalum (Ta) and niobium (Nb) content across samples, reflecting the mineralogical diversity within the columbite–tantalite series. Samples 3, 4, 5, 7, 9, and 10 have high Ta contents (above 43%), positioning them toward the tantalite end-member and making them more valuable for tantalum extraction. In contrast, samples 1, 2, and 6 have higher Nb than Ta, aligning them more closely with the columbite variety, which is better suited for niobium recovery. The Fe and Mn distribution further refines classification, with higher Mn suggesting manganotantalite or manganocolumbite tendencies, and higher Fe pointing to ferrocolumbite or ferrotantalite types.

The other elements, representing minor elements such as Ti, remain relatively low in most samples, indicating clean mineral assemblages favourable for processing. High Ta–Nb values, where Ta-dominant samples directly enhance economic potential, as tantalum is a strategic metal in electronics, aerospace, and energy industries. The Fe and Mn proportions also have metallurgical implications, influencing magnetic susceptibility and density, which in turn affect beneficiation techniques. Overall, the dataset reflects a mix of high-grade tantalite ores and niobium-rich varieties, providing multiple avenues for economic extraction.

4. Conclusion

The geophysical survey successfully delineated subsurface resistivity variations across all four profiles, identifying mineralised zones primarily within conductive layers with resistivity ranging from approximately 11.9 Ω · m to 186 Ω · m at depths between 1.25 m and 35 m. High-resistivity bedrock or intrusions exceeding 2,000 Ω · m marked the lower boundaries of mineralisation, indicating that tantalite deposits are hosted in weathered troughs, conductive overburden, or vertical to sub-vertical structures above competent basement rocks. These resistivity contrasts provided clear geological controls for targeting mineral accumulation zones.

The geochemical analysis of ten rock samples confirmed the presence of tantalite-series minerals, with samples 3, 4, 5, 7, 9 and 10 showing tantalum contents above 43%, positioning them as high-value tantalum ores. Samples 1, 2 and 6 exhibited higher niobium than tantalum, aligning with the columbite variety. The consistent association of tantalum with niobium, iron, and manganese, along with low concentrations of minor elements, indicates clean mineral assemblages favourable for processing. Together, the geophysical and geochemical results define a coherent mineralised system with significant economic potential for tantalum extraction within the first 30 m of the subsurface.

References

[1] Kraft, M., Flores, J. R., Klopper, W., Kappes, M. M., and Schooss, D. (2021). Structures of small tantalum cluster anions: Experiment and theory. The Journal of Physical Chemistry A, 125, 3135–3145. https://doi.org/10.1021/acs.jpca.1c01250

[2] Mackay, D. A., and Simandl, G. J. (2014). Geology, market and supply chain of niobium and tantalum - a review. Mineralium Deposita, 49(8), 1025–1047.

[3] Norooz, R., Nivorlis, A., Olsson, P.-I., Gunther, T., Bernstone, C., and Dahlin, T. (2024). Monitoring of Älvkarleby test embankment dam using 3D electrical resistivity tomography for detection of internal defects. Journal of Civil Structural Health Monitoring, 14, 1275–1294. https://doi.org/10.1007/s13349-024-00785-x

[4] Ochola, K. (2021). Application of geophysical exploration methods in mapping gold mineralisation zones. Case study: Makina prospect in the Busia-Kakamega greenstone belt, S.E. Uganda. [Doctoral dissertation, University of Nairobi].

[5] Pacanowski, G., Maslakowski, M., & Lejzerowicz, A. (2022). Practical aspects of field work carried out by electrical resistivity tomography. Archives of Civil Engineering, 68(4). DOI:10.24425/ace.2022.143041

[6] Simmons, W. B., Webber, K. L., & Falster, A. U. (2023). Pegmatites: Rocks and Minerals, Vol 99, No 1, 18-32. https://doi.org/10. 1080/00357529.2023.2253098